

Interaction effects and quantum phase transitions in topological insulatorsChristopher N. Varney,^{1,2} Kai Sun,^{2,3} Marcos Rigol,¹ and Victor Galitski^{2,3}¹*Department of Physics, Georgetown University, Washington, DC 20057, USA*²*Joint Quantum Institute and Department of Physics, University of Maryland, College Park, Maryland 20742, USA*³*Condensed Matter Theory Center, Department of Physics, University of Maryland, College Park, Maryland 20742, USA*

(Received 19 July 2010; revised manuscript received 26 August 2010; published 28 September 2010)

We study strong correlation effects in topological insulators via the Lanczos algorithm, which we utilize to calculate the exact many-particle ground-state wave function and its topological properties. We analyze the simple, noninteracting Haldane model on a honeycomb lattice with known topological properties and demonstrate that these properties are already evident in small clusters. Next, we consider interacting fermions by introducing repulsive nearest-neighbor interactions. A first-order quantum phase transition was discovered at finite interaction strength between the topological band insulator and a topologically trivial Mott insulating phase by use of the fidelity metric and the charge-density-wave structure factor. We construct the phase diagram at $T=0$ as a function of the interaction strength and the complex phase for the next-nearest-neighbor hoppings. Finally, we consider the Haldane model with interacting hard-core bosons, where no evidence for a topological phase is observed. An important general conclusion of our work is that despite the intrinsic nonlocality of topological phases their key topological properties manifest themselves already in small systems and therefore can be studied numerically via exact diagonalization and observed experimentally, e.g., with trapped ions and cold atoms in optical lattices.

DOI: [10.1103/PhysRevB.82.115125](https://doi.org/10.1103/PhysRevB.82.115125)

PACS number(s): 71.10.Fd, 03.65.Vf, 05.30.Fk, 21.60.Fw

I. INTRODUCTION

The conventional definition of a topological insulator (TI) relies on an analysis of noninteracting band structures and from the mathematical point of view represents topological classification of the spectrum of matrix Hamiltonians.¹⁻⁷ While this approach is nongeneralizable to interacting systems, it is clear that they may exhibit physical phenomena associated with nontrivial topological spectra. Qi and co-workers recently suggested a more general definition of a topological insulator, potentially suitable to interacting systems, which is defined as a state where charged carriers give rise to axion electrodynamics with a nontrivial electromagnetic coupling term.^{7,8} One possible approach would be to use the Volovik formula for topological indices, which involves exact Green's functions.⁹ In addition, a technique utilizing a Green's functions formula for time-reversal invariant topological insulators was recently presented.¹⁰ Finally, the topological properties can also be studied via explicit analysis of the edge states and the density-of-states (DOS) spectrum with an eye on the localized boundary modes that would connect bands across a gap.

Interacting topological models are expected to be even richer than the noninteracting systems and may host a variety of different phases and phase transitions. However, despite this expected rich variety of phenomena and fundamental interest, the effect of interactions in topological insulators has remained largely unexplored and the current knowledge of this issue is rather limited.¹¹⁻¹⁶ The existing open questions include the following. (i) Can topological properties be tuned by interactions? (ii) What is the nature of the quantum phase transitions separating phases from different topological classes? (iii) Are topological Mott insulators possible, where the nontrivial phase would arise entirely due to interactions? And an even more provocative question: (iv) can topological

Mott insulators exist in bosonic systems? The main difficulty in addressing these questions is that they all involve strong correlation physics, where essentially no quantitatively reliable analytical methods exist. The usefulness of quantum Monte Carlo techniques¹⁷ is expected to be limited by the infamous sign problem.^{18,19} The last resort resides in exact diagonalization methods and other unbiased numerical techniques, which are limited to small system sizes as the dimension of the Hilbert space grows exponentially with system size. The latter circumstance is important, particularly because topological phases involve nonlocal effects and it is not clear if they survive in small systems [e.g., due to detrimental effect of tunneling between the edge states in finite lattices with open boundary conditions (OBC)].

In this paper, we employ the Lanczos algorithm^{20,21} to calculate the exact ground-state wave function of interacting lattice models which are known or expected to have a topological ground state. We focus our analysis on four observables that provide unique insights into the properties of these lattice models. The topological phase is examined with the local density of states (LDOS), which we determined for both open and periodic boundary conditions (PBC). As we will discuss in detail below, the key topological features are still discernible in relatively small clusters (at least in two-dimensional lattices), which are within the reach of exact diagonalization techniques. The next two observables of interest are the edge currents and the structure factor, which we define carefully in the next section. The final observable of interest is the ground-state fidelity metric g , defined below in Eq. (10). The fidelity metric is related to the rate of change in the overlap between the ground-state wave function in Hamiltonians that differ by a small control parameter. The ground-state fidelity was originally studied in quantum information theory and has been shown to be a sensitive indicator of quantum phase transitions.²²⁻³¹ In conjunction with the structure factor, the fidelity metric is used to characterize the

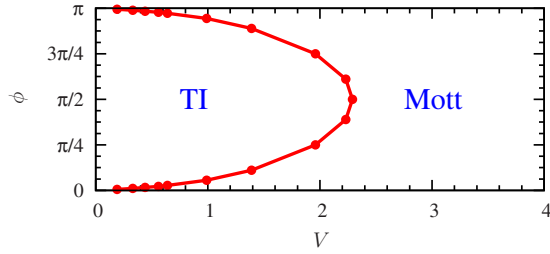


FIG. 1. (Color online) Schematic V - ϕ phase diagrams for spinless fermions in the Haldane model at half filling. For $0 < \phi < \pi$, the system is a topological insulator (TI) at weak coupling and becomes a Mott insulator at finite interaction strengths via a first-order phase transition. At $\phi=0$ and $\phi=\pi$, the TI phase is not possible. Instead, the phase at weak coupling is a semimetal. The points in the phase boundary were calculated for a 24-site cluster (24D).

nature of the transition from the topological insulator to the topologically trivial Mott insulator.

To test the feasibility of the Lanczos algorithm and to explore the main questions, we chose the Haldane model on a honeycomb lattice, but with nearest-neighbor repulsive interactions. The noninteracting base model is known to have a simple topological phase transition to a trivial band insulator,¹ which can be tuned by adjusting a staggered chemical potential, M . Moreover, in the limit of weak interaction strengths, the bulk gap and nontrivial topology are known to persist.^{32–34} This allows us to calibrate the techniques on the noninteracting and weakly interacting fermion model, whose topological ground state is known and well understood. The main conclusion of this initial analysis is that the local density of states for the bulk and the edge are the most useful metrics to probe the topological nature of the ground state. On the other hand, we find that the existence of the chiral edge currents may be misleading, as those may be present even in topologically trivial phases and their origin and stability cannot be determined just by looking at the current texture in the ground state. Indeed, this result has been independently verified for noninteracting systems.³⁵

With these caveats in mind, we analyze the strongly interacting Haldane model with spinless fermions. The model is characterized by four independent parameters: nearest-neighbor hopping amplitude, t_1 , next-nearest-neighbor hopping amplitude, t_2 , and its complex phase ϕ , and the nearest-neighbor coupling, V . We limit our analysis of the interacting model to the case of zero staggered potential, $M=0$, which apart from the trivial case of $\phi=0$ (which is a semimetal) is guaranteed to be a topological insulator for $V \ll t_{1,2}$. We find that as V is increased, the system undergoes a topological quantum phase transition into a topologically trivial Mott insulator with the critical interaction strength $V_c(\phi) = V_c(\pi - \phi)$ monotonically increasing from $V_c(\pi/180) = 0.19t_1$ to $V_c(\pi/2) = 2.29t_1$ within half a period (see Fig. 1). The appearance of the Mott insulator is not surprising, but it is not *a priori* clear if the Mott transition must always coincide with the loss of the topological order or if there are two separate transitions. Below, we show compelling evidence that the former scenario is the one realized in this model, that there is a single first-order quantum phase transition at intermediate couplings.

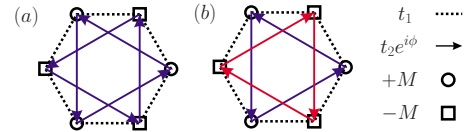


FIG. 2. (Color online) Illustration of (a) the Haldane model and (b) the modified Haldane Hamiltonian. In (b), the direction of positive complex phase in the next-nearest-neighbor hopping on the sublattice denoted by the squares is reversed.

Finally, we populated the Haldane honeycomb lattice with interacting hard-core bosons in the hope that a phase with nontrivial topological properties may emerge in this Bose-Hubbard model at intermediate couplings. However, it was found not to be the case. At half filling, the system remains a trivial superfluid until considerable values of nearest-neighbor repulsion parameter is reached, at which point a superfluid-to-Mott-insulator transition takes place. However, it is not a topological Mott insulator because the DOS shows no evidence of an edge state crossing the Hubbard gap. Because this hard-core boson model has interesting features beyond the focus of this paper, we defer a full discussion of its properties for future work.³⁶

The remainder of this paper is structured as follows. In Sec. II we define the model and the key measurements used to characterize the ground state: local density of states, structure factor, and the fidelity metric. In addition, the Lanczos algorithm is briefly discussed. In Sec. III, we examine the exactly solvable noninteracting Haldane model and show that topological phases can be observed on small lattices. Next, we present the results for interacting systems in Sec. IV, with Sec. IV A devoted to spinless fermions and Sec. IV B to hard-core bosons. The main results and outlook are summarized in Sec. V.

II. MODEL AND MEASUREMENTS

The Haldane Hamiltonian¹ is a well-known model of free fermions that features the anomalous quantum Hall state. In real space, the Hamiltonian is given by

$$H_{\text{Haldane}} = -t_1 \sum_{\langle ij \rangle} (c_i^\dagger c_j + c_j^\dagger c_i) - t_2 \sum_{\langle\langle ij \rangle\rangle} (e^{i\phi_{ij}} c_i^\dagger c_j + e^{-i\phi_{ij}} c_j^\dagger c_i) + M \sum_i (-1)^{\sigma(i)} n_i, \quad (1)$$

where c_i^\dagger (c_i) represent the fermion creation (annihilation) operators at site i and $n_i = c_i^\dagger c_i$ is the corresponding number operator. Here M is a staggered potential that breaks the symmetry between the two sublattices of a honeycomb lattice, indicated by odd or even values of $\sigma(i)$, and t_1 (t_2) are the nearest-neighbor (next-nearest-neighbor) hopping amplitudes. The next-nearest-neighbor hopping term has a complex phase $\phi_{ij} = \pm \phi$. In the Haldane model, the origin of this term is a varying magnetic field that has zero net flux in a given hexagon. This is illustrated in Fig. 2(a), where the sign of the complex phase is positive in the direction of the vector between next-nearest-neighbor sites. In Fig. 2(b), we show a slightly modified version of the Hamiltonian, which differs

from the Haldane Hamiltonian in that the direction of positive complex phase on one sublattice is reversed.

In this paper, we investigate the properties of the Haldane model for interacting particles (spinless fermions or hard-core bosons) at half filling. The Hamiltonian $H = H_{\text{Haldane}} + H_{\text{int}}$, where

$$H_{\text{int}} = V \sum_{\langle ij \rangle} n_i n_j \quad (2)$$

and V describes a repulsive nearest-neighbor interaction.

To study the interacting system, we utilize the Lanczos algorithm.²⁰ (Details of the algorithm in the context of Hermitian matrices can be found in Ref. 21.) The main advantage of this technique is that it provides extremely accurate information about the ground-state wave function for interacting quantum systems. Unfortunately, memory limitations restrict the size of the clusters that can be studied. For the Hamiltonians of interest in this paper, we consider various clusters with periodic boundary conditions. The largest cluster studied has 30 sites, which at half filling has a Hilbert space of $30!/(15!)^2 \sim 1.55 \times 10^8$, near the limit of what is accessible on present-day computers. We also consider one cluster with 24 sites and open boundary conditions, which is used to study surface related effects. As discussed above in Sec. I, the ground-state wave function determines the topological nature of a quantum system. More importantly, as we will show in Sec. III, the topological properties in the anomalous quantum Hall system can be observed for small systems with only 24 sites (or even smaller). These important features of the topological insulator make the Lanczos algorithm a suitable tool in the study of the topological properties.

As a vital feature of the Haldane model, there is no net flux in each unit cell of the lattice. The absence of net flux turns out to be crucial in the study of the topological edge states. As we implement the open boundary condition, this could introduce a local flux near the boundary. This local flux induces Faraday currents at the edge, which hybridize with the topological edge currents and prevent a clear observation of the topological edge states. Thus, it is crucial for the edge configuration to be chosen carefully to avoid the net flux at the edge. In the numerical works reported here, we removed the next-nearest-neighbor hopping terms between the sites on the edge that do not pass through a hexagon to preserve this property.

One of the distinguishing characteristics of a topological insulator is the presence of a (topologically protected) conducting edge state with an insulating bulk. The LDOS can be measured via scanning tunneling microscopy in conventional condensed matter systems.³⁷ For a noninteracting system, it is defined as

$$N_i(\omega) = \sum_n |\langle i | \Psi_n \rangle|^2 \delta(\omega - E_n), \quad (3)$$

where $|\langle i | \Psi_n \rangle|^2$ is the weight of the state $|\Psi_n\rangle$ with a particle in site i . In the Lanczos algorithm, the local density of states is given by

$$N_i(\omega) = \begin{cases} \sum_n |\langle \Psi_{n-1} | c_i | \Psi_n \rangle|^2 \delta[\omega - (E_{n-1} - E_n)] & \omega < \mu \\ \sum_n |\langle \Psi_n | c_i^\dagger | \Psi_{n+1} \rangle|^2 \delta[\omega + (E_n - E_{n+1})] & \omega > \mu, \end{cases} \quad (4)$$

where $|\Psi_n\rangle = \sum_m a_m^n |\phi_m^n\rangle$ is the n th eigenvector with particle number N and energy eigenvalue E_n and $|\phi_m^n\rangle$ are the orthonormalized vectors determined in the Lanczos procedure. In addition, it can easily be shown³⁸ that

$$|\langle \Psi_{n'} | \hat{O} | \Psi_n \rangle|^2 = |a_0^n|^2 \langle \Psi_n | \hat{O}^\dagger \hat{O} | \Psi_n \rangle, \quad (5)$$

where $n' = n \pm 1$. Further details on dynamical properties in Lanczos can be found in Refs. 38–40.

To better understand the edge states in our models, we considered the current on every bond in the lattice. Between sites m and n , the magnitude of the density current J_{mn} is defined to be⁴¹

$$J_{mn} = \frac{iqr_{mn}}{\hbar} (t_{mn} c_m^\dagger c_n - t_{nm} c_n^\dagger c_m), \quad (6)$$

where q is the charge carried by a particle and r_{mn} is the magnitude of the position vector between the two sites.

For large repulsive interaction strengths, the topological insulator will give way to a trivial charge-density-wave (CDW) insulator through a topological phase transition. In the limit $V \rightarrow \infty$, the ground state will be a perfect CDW, where one of the two sublattices is occupied while the other is empty, leaving lattice translational symmetry intact but breaking reflection symmetry.⁴² The correlation function that describes the CDW phase is

$$C(\mathbf{r}_i - \mathbf{r}_j) = \langle (n_i^a - n_i^b)(n_j^a - n_j^b) \rangle, \quad (7)$$

where n_i^a and n_i^b are the number operators on sublattice a and b in the i th unit cell, respectively. The corresponding structure factor is

$$S(\mathbf{k}) = \frac{1}{N} \sum_{i,j} e^{i\mathbf{k} \cdot (\mathbf{r}_i - \mathbf{r}_j)} C(\mathbf{r}_i - \mathbf{r}_j). \quad (8)$$

Because the long-range order is diagonal, $S(\mathbf{k})$ will be maximal at $\mathbf{k} = 0$ and we define $S_{\text{CDW}} \equiv S(\mathbf{k} = 0)$.

In order to study this quantum phase transition, we introduce an observable related to the fidelity F . Let $|\Psi_0(V)\rangle$ be the ground state of $H(V)$ and $|\Psi_0(V + \delta V)\rangle$ be the ground state of $H(V + \delta V)$. The fidelity $F(V, \delta V)$ is simply the overlap between these two wave functions

$$F(V, \delta V) = |\langle \Psi_0(V) | \Psi_0(V + \delta V) \rangle|. \quad (9)$$

The fidelity metric g is a dimensionless, intensive quantity and can be defined as

$$g(V, \delta V) \equiv \frac{2}{N} \frac{1 - F(V, \delta V)}{(\delta V)^2}, \quad (10)$$

where N is the number of sites. For finite-size systems, a decrease in the fidelity is a precursor to a quantum phase transition. This corresponds to a peak in the fidelity metric, which should diverge in the limit $N \rightarrow \infty$ for a second-order

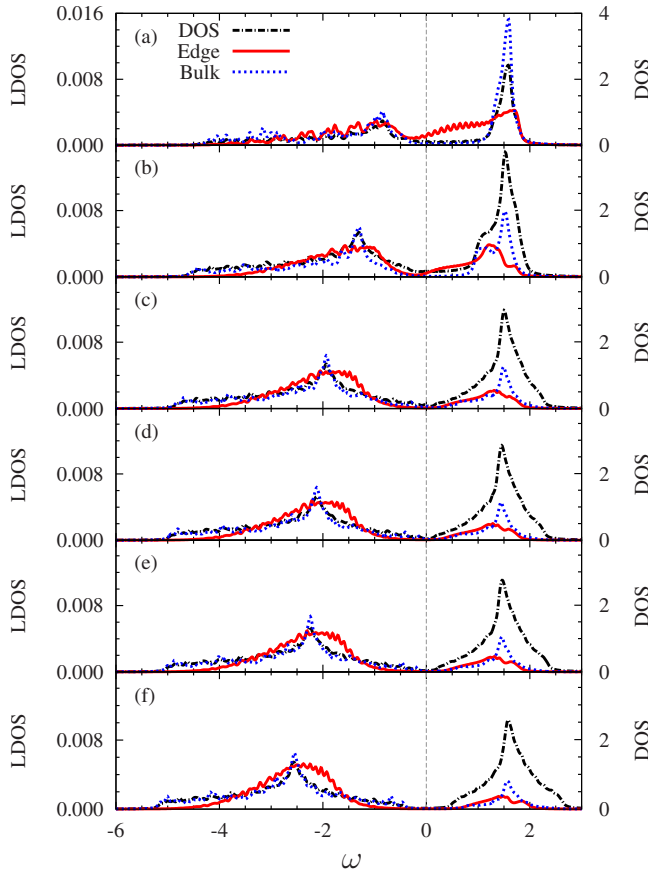


FIG. 3. (Color online) Total density of states and local density of states in the Haldane model for a site on the edge and in the bulk for (a) $M=0.0$, (b) $M=0.5$, (c) $M=1.0$, (d) $M=1.1$, (e) $M=1.2$, and (f) $M=1.5$. The calculations were performed on a $N=420$ -site cluster with $t_1=1.0$, $t_2=0.3$, and $\phi=\pi/4$. The gap in the edge states opens at $M_c=1.1$. The vertical, gray line indicates the chemical potential.

phase transition. For a transition to the CDW phase, this will coincide with a peak in $S(\mathbf{k}=0)$, which will similarly diverge. The fidelity metric also tracks level crossings well. At a level crossing, the wave functions $|\Psi(V)\rangle$ and $|\Psi(V+\delta V)\rangle$ will be very different. Because the overlap between the two states is negligible, the fidelity metric is sharply peaked. This, in conjunction with a jump in the structure factor $S(\mathbf{k}=0)$, will distinguish a first-order phase transition. In the calculations that follow, we take $\delta V=10^{-4}$, which is sufficiently small to ensure results consistent with $\delta V \rightarrow 0$.

III. NONINTERACTING SYSTEMS

We first study the noninteracting fermions, which are exactly solvable, to compare our numerical results with the known solution. In addition, this limit allows for the study of large clusters and we can carefully address whether the small clusters that are accessible with the Lanczos algorithm are suitable for observation of a topological insulator.

As Haldane was able to show previously,¹ there is a phase transition between the topological insulator and the topologically trivial charge insulator as one increases the value of M . For M below the critical value of $M_c=3^{3/2}t_2 \sin \phi$, the sys-

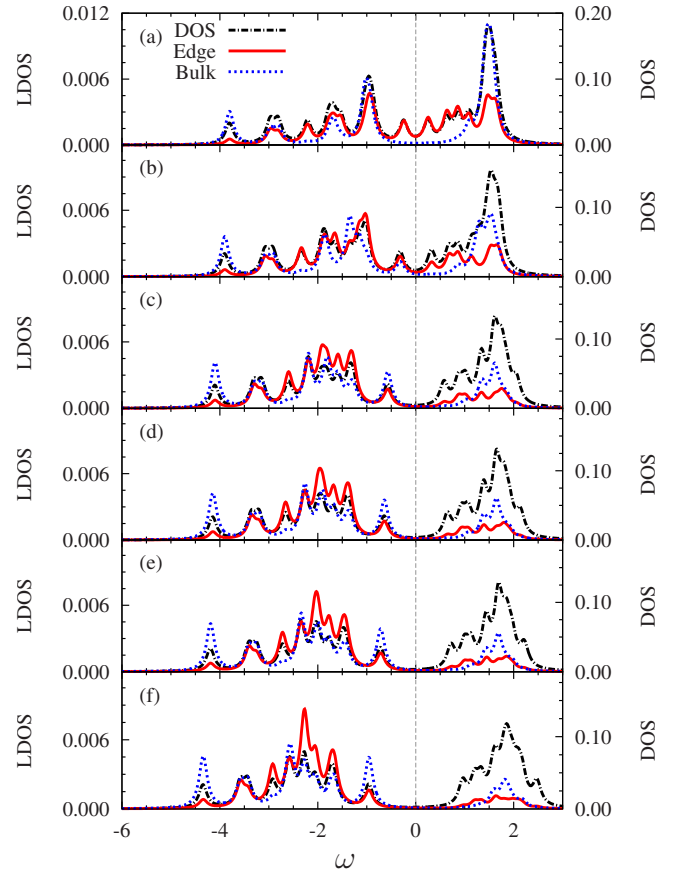


FIG. 4. (Color online) Total density of states and local density of states in the Haldane model for a site on the edge and in the bulk for (a) $M=0.0$, (b) $M=0.5$, (c) $M=1.0$, (d) $M=1.1$, (e) $M=1.2$, and (f) $M=1.5$. The calculations were performed on a $N=24$ -site cluster with the same parameters as in Fig. 3. The vertical, gray line indicates the chemical potential. Because of the finite size, the gap opens at smaller M and is, in general, larger than in Fig. 3.

tem is a topological insulator with an insulating bulk and a chiral metallic edge. As M approaches M_c , the insulating gap in the bulk decreases and closes at $M=M_c$ while the system becomes a semimetal. If one further increases M , an insulating gap develops in both the bulk and the edge. However, this insulator is topologically trivial and there are no gapless edge states with topological protection.

Unlike an ordinary phase transition, this transition was beyond the framework of the Landau's theory of phase transitions. The two phases discussed above cannot be distinguished by any local parameter and no symmetry was broken across this transition. As a result, Landau's free energy cannot be defined. The only distinction between these two phases are their topological property, which is described by a topological index known as the Chern number.^{1,43,44} Experimentally, one can distinguish these two phases by their edge properties. We also emphasize here that this phase transition shows no discontinuity for any thermodynamical quantity and a similar example of a topological transition is the transition between the strong and weak pairing in p_x+ip_y superconductors (at least within the mean-field treatment).^{44,45}

This topological transition can be observed by measuring the local density of states [Eq. (3)]. Since we deal here with

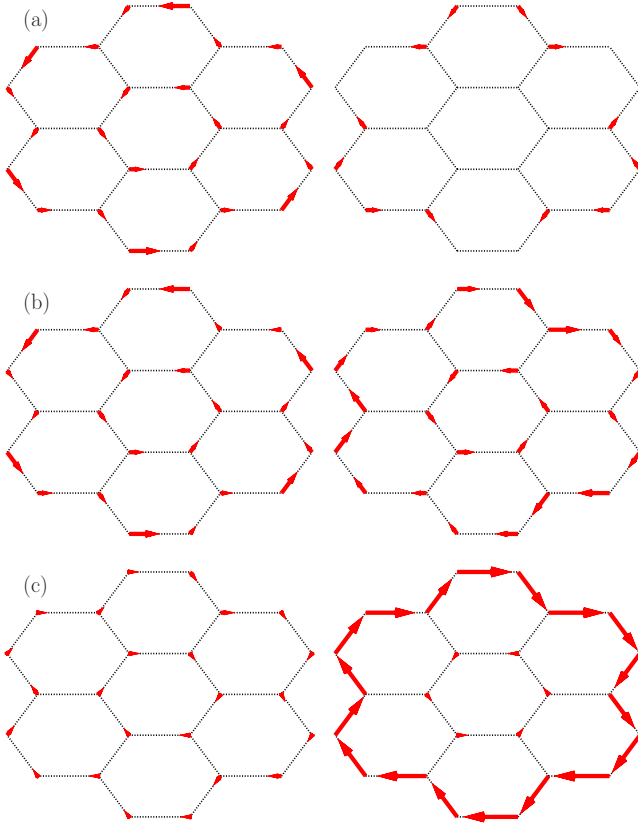


FIG. 5. (Color online) Nearest-neighbor currents for the Haldane (left) and modified Haldane (right) Hamiltonians on a $N=24$ -site cluster and parameters $t_1=1.0$, $t_2=0.3$, and $\phi=\pi/4$ with (a) $M=0$, (b) $M=0.10$, and (c) $M=1.5$. In the modified Haldane model, a nonzero circulating current exists for $M \neq 0$, i.e., the moment chiral symmetry is broken.

finite-size systems, the energy spectrum is discrete. To compensate for this, we have broadened the delta function peaks with a Lorentzian of width $\gamma=0.01t_1$. As shown in Fig. 3, for small M , the LDOS has no energy gap for a site on the edge, indicating clearly a metallic edge. However, for the bulk site, the same spectrum becomes gapped, reflecting an insulating bulk.

To estimate the effects of finite-sized systems on this transition, we reduced the size of the cluster down to 24 sites (12 unit cells). In Fig. 4, the bulk gap and the gapless edge states can still be observed, indicating that the topological property of the anomalous quantum Hall state is robust with regard to finite-sized clusters. A similar effect was also observed in a system fundamentally different from the model studied here. As reported in Ref. 46, the topological ordering in the Kitaev model⁴⁷ was observed for small system sizes. While the topological ordering found by Chen *et al.* has little direct relation with the results presented here, the fact that the same phenomenon is observed in these two systems suggests that robustness against finite-size effects might be a common property shared by different topological states of matter.

We also computed the nearest-neighbor current [Eq. (6)] in the system, which is shown for $M=0, 0.1$, and 1.5 in Fig. 5 (next-nearest-neighbor currents are not shown because they are an artifact of the complex hopping in the Hamiltonian

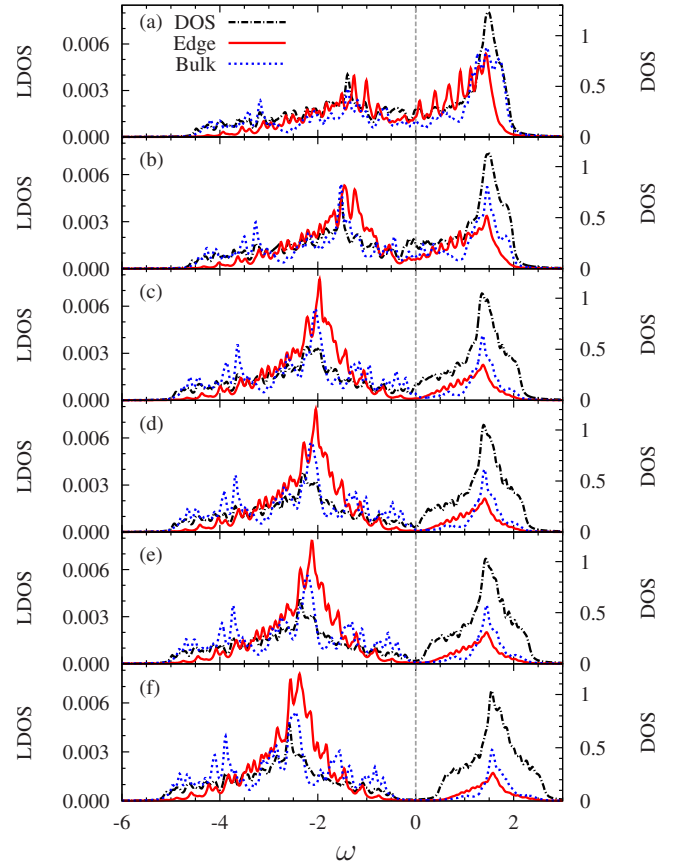


FIG. 6. (Color online) Total density of states and local density of states in the modified Haldane model for a site on the edge and in the bulk for (a) $M=0.0$, (b) $M=0.5$, (c) $M=1.0$, (d) $M=1.1$, (e) $M=1.2$, and (f) $M=1.5$. The calculations were performed on a $N=420$ -site cluster with $t_1=1.0$, $t_2=0.3$, and $\phi=\pi/4$. The gap in the edge states opens at $M_c=1.1$. The vertical, gray line indicates the chemical potential.

and exist for all parameters). Note that the topological state has a clear chiral edge current (rotating in the clockwise direction) while the current in the bulk is negligible. However, in the topologically trivial insulator with $M > M_c$, the chiral current remains until M becomes large. This is because Haldane's model explicitly breaks chiral symmetry, which allows for a rotating edge current. Due to this effect, by measuring only the edge current, it is not sufficient to distinguish the topologically trivial insulator from the topological insulator. Indeed, the proper means of distinguishing the topological state is via the LDOS.

For comparison purposes, we also studied a modification to Haldane's model [Fig. 2(b)], where the two sublattices have opposite flux patterns. This model is topologically trivial in all of the parameter regimes. For $M < M_c$, the system is a conductor (a Fermi liquid) at half filling but becomes a topologically trivial insulator for $M > M_c$. At the transition point $M=M_c$ (which is identical to the transition point in Haldane's model), the system is a semimetal. This transition was observed clearly in the LDOS (Fig. 6). In particular, the insulating phase with $M > M_c$ was found to be gapped both in the bulk and on the edge, which, as expected, signifies a topologically trivial insulator. Moreover, the same

behavior can be found even for the small clusters with only 24 sites (not shown).

Although the modified Haldane's model is topologically trivial, this system has its own significance in the study of the anomalous Hall effect. As in the Haldane's model described previously, this model also has no net magnetic flux. However, the flux pattern breaks the chiral and time-reversal symmetries for any $M \neq 0$, even in the absence of the a net magnetic flux. These symmetry properties are in close analogy to the (nonquantized) Hall effect, although the magnetic field is zero after averaging over each unit cell in this case. Due to this similarity, the conducting phase in the modified Haldane's model with $0 < M < M_c$ is referred to as an anomalous Hall state.^{43,48} This anomalous Hall effect can be easily observed by looking at the currents in the system (see panels on right side of Fig. 5). At $M=0$, the chiral symmetry is preserved, and the current on the left and right edges flows in opposite direction in order to preserve the chiral symmetry. However, for $M > 0$, the ground state of the system is the metallic anomalous Hall state, which breaks the chiral symmetry. Now, the currents at the opposite edge will not cancel each other. Instead, they flow in the same direction and form a rotating current circling around the system. We emphasize here that this edge current is not related with a nontrivial topological structure in the ground-state wave function, and it only reflects the broken chiral symmetry.^{43,48,49}

IV. INTERACTING SYSTEMS

A. Spinless fermions

Having shown that the topological insulator phase can be distinguished on small lattices, we now consider the properties of interacting systems. In this section, we consider spinless fermions with repulsive nearest-neighbor interactions (hard-core bosons are discussed in Sec. IV B). In the discussion that follows, we present detailed results for the parameters $t_1=1.0$, $t_2=0.3$, $\phi=\pi/4$, and $M=0$ before discussing the results for general ϕ .

At the noninteracting limit, we have shown above that, at $M=0$, the system is a topological insulator and the two sublattices have the same occupation number. In the strong-coupling limit $V \rightarrow \infty$, however, the particles will all go to one of the two sublattices to avoid the energy penalty for occupying two neighboring sites. At half filling, one sublattice is fully filled while the other one is empty, resulting in a CDW insulating phase. Note with the formation of the CDW, translational symmetry remains but inversion symmetry was spontaneously broken. Hence, we conclude that the system goes through a quantum phase transition as V is increased. More interestingly, the insulating phase in the weak-coupling limit is signified by a nontrivial Chern number.^{1,43,44} However, the CDW phase in the strong-coupling limit has a trivial Chern number ($C=0$) and is topologically trivial. Therefore, the topology of the ground-state wave function changes from nontrivial to trivial as V increases. This change in topology is referred as a topological transition. Within the current knowledge of the topological insulators, it is not clear whether the quantum phase transition and the topological transition are, in general, two separate transitions or if

they coincide to become a single phase transition.

We first consider the topological transition by examining the LDOS at the edge and in the bulk. In Fig. 7, we show local currents (left) and the local density of states (right) on a 24-site cluster with open boundary conditions for several interaction strengths. At $V=0$ [Fig. 7(a)], the system is a topological insulator, evidenced by the bulk insulating gap and the metallic local density of states on the edge. The circulating current on the edge is also consistent with the quantum Hall state. As the interaction strength is increased, the gap in $N_{\text{bulk}}(\omega)$ closes while the states near the chemical potential in $N_{\text{edge}}(\omega)$ are depleted. For $V=2, 3$, and 4 [Figs. 7(c)–7(e)], the edge states are fully gapped and the system is a trivial insulator. The local density of states in this phase is characterized by a near complete depletion of the bulk states closest to the gap in the upper band, effectively resulting in a larger insulating gap in the bulk than on the edge. The topological transition takes place at $V_T \approx 2$. Finally, we note that the trivial insulator at intermediate coupling is characterized by small but nonzero edge currents that travel in the opposite direction from the edge currents in the topological insulating phase. In the limit of $V \gg t_1$, the edge currents vanish.

Next, we consider the nature of the quantum phase transition which leads to the spontaneous breaking of inversion symmetry. Here, the momentum space properties of the cluster are vital to the type of transition observed. The noninteracting band structure for this Hamiltonian features a Dirac cone at the zone corner $K=(2\pi/3, 2\pi/\sqrt{3})$. For an infinite system, this will always be a valid momentum point, whereas for small clusters this is not generally the case. Because the surface states in the band structure pass through this point in reciprocal space, the order of the transition has a clear dependence on the choice of clusters. This is reflected in the fidelity metric and the scaled CDW structure factor $N^{-\gamma/2\nu} S_{\text{CDW}}$, which are shown in Fig. 8 for clusters from $N=16$ to $N=30$ sites with periodic boundary conditions (see the Appendix for more details on the cluster shapes). If one studies clusters with a reciprocal space that does not contain the zone corner, then a broad maximum in the fidelity metric and a crossing of the scaled structure factor is observed at $V \approx 2.0$. On just this information, one would conclude that there is a second-order phase transition at this interaction strength. However, clusters that contain the K point (18A, 18C, 24C, 24D, and 30A) exhibit markedly different behavior. Instead, we find that the fidelity metric exhibits a very large and sharp peak (18C, 24C, and 30A) or discontinuity (18A and 24D) at $V \approx 2.0$. Furthermore, the CDW structure factor exhibits a jump at this interaction strength, indicating a first-order phase transition. Indeed, when we examine the first derivative of the structure factor [see Fig. 8(b) inset], there is removable discontinuity at $V_c \approx 2.0$, which indicates that the topological transition and the quantum phase transition occur at the same interaction strength.

For the clusters that do not contain the K point, the quantum phase transition is a conventional one (in contrast to the topological phase transitions discussed above). Because the inversion operator and the identity operator form a Z_2 group, the symmetry-breaking pattern of this quantum phase transition belongs to the Z_2 (also known as Ising) universality class. If the transition is second order, it is then expected to

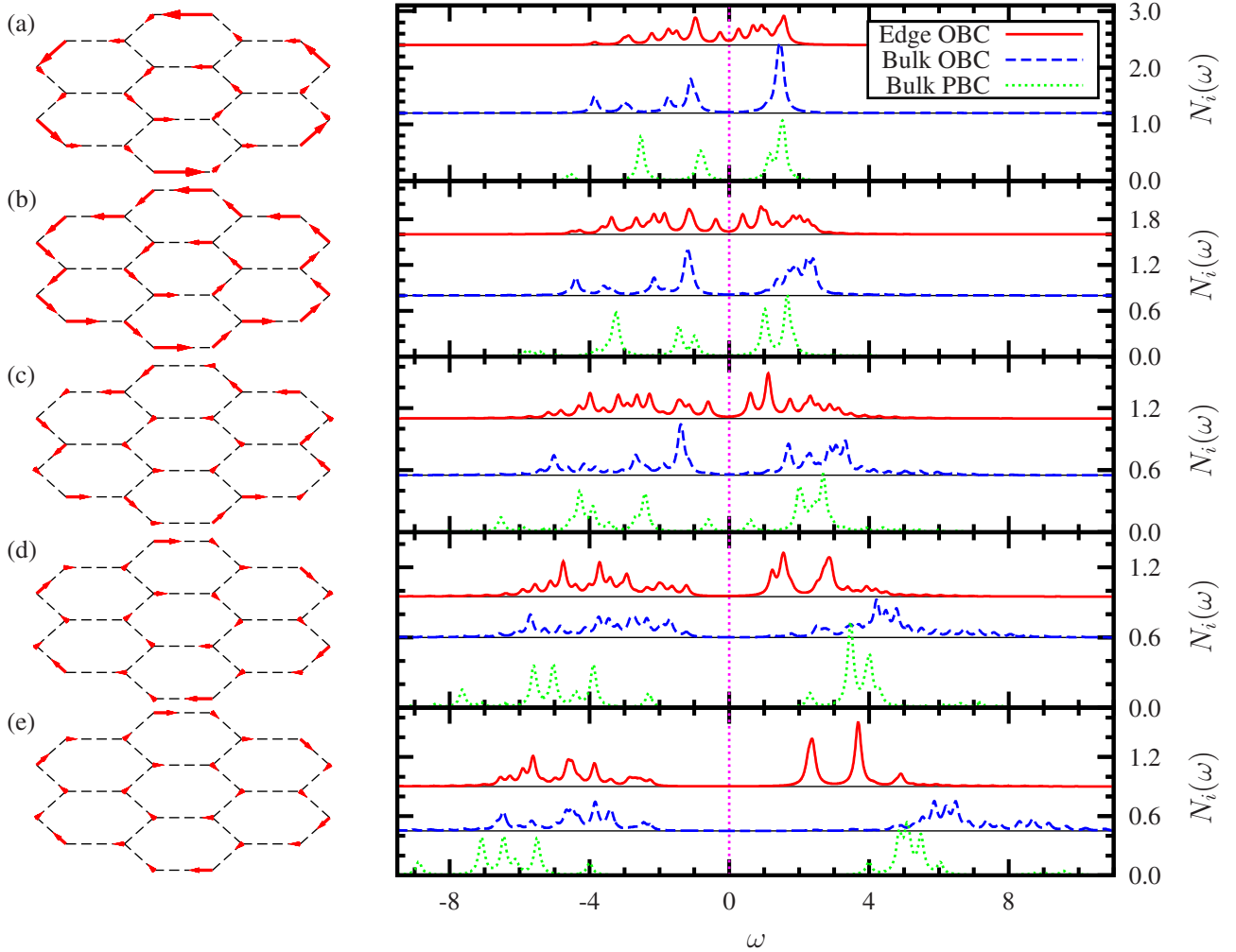


FIG. 7. (Color online) Nearest-neighbor currents (left) for spinless fermions on a 24-site cluster with OBC, $t_1=1.0$, $t_2=0.3$, $\phi=\pi/4$, and interaction strengths (a) $V=0$, (b) $V=1$, (c) $V=2$, (d) $V=3$, and (e) $V=4$. Local density of states (right) for the edge (OBC) and the bulk (shown for both OBC and PBC). The zeros of $N_{\text{edge}}(\omega)$ and $N_{\text{bulk,OBC}}(\omega)$ are shifted upward for clarity, and the frequency ω is shifted so that the chemical potential is at $\omega=0$ (which is also indicated by the dashed vertical line). The delta function is broadened by a Lorentzian of width $\gamma=0.01t_1$.

follow the scaling relation of the Ising model in $d+z$ dimensions. Here $d=2$ is the spatial dimension and z is the dynamic critical exponent, which is usually a positive integer indicating how many spatial dimensions the time dimension shall be counted as.⁵⁰ For $z=1$, the critical point follows the three-dimensional (3D) Ising scaling, for $z=2$ and above, the exponents are the mean-field exponents.^{51,52}

We expect that the structure factor will scale according the following rule:

$$N^{-\gamma/2\nu} S_{\text{CDW}} = f[(V - V_c)N^{1/2\nu}], \quad (11)$$

where N is the number of sites and $\gamma=\nu(2-\eta)$. For a 3D Ising model⁵¹ (corresponding to the case of $z=1$), $\nu=0.7$ and $\eta=0.04$ while in four dimensions (4D) and above^{52,53} ($z \geq 2$), $\nu=0.5$ and $\eta=0$. As the proper value of z is still an open question, we show the rescaled structure factor $N^{-\gamma/2\nu} S_{\text{CDW}}$ as a function of interaction strength for both of these cases in Fig. 9. If the transition is second order, the set of curves will converge at the quantum critical point $V=V_c$.

Here, the critical point obtained in both cases remains almost unchanged. Moreover, we show the universal scaling relation, Eq. (11), in the insets of Fig. 9 and observe the same qualitative behavior for both $z=1$ and $z=2$. As there is no discernible qualitative difference between the scaling with $z=1$ and $z=2$, it is clear that higher order corrections in the finite-size scaling are relevant. For the largest system size shown in Fig. 9, the linear system size is $L=N^{1/2} \approx 4.9$. Thus, significantly larger system sizes need to be studied in order to properly determine the value of z .

In Fig. 1(a), we present a schematic phase diagram for this model in the $V-\phi$ plane. Note that the phase boundary shown in the figure is determined for a 24-site cluster from the maximum in the derivative of S_{CDW} [see Fig. 8(b) inset]. At $\phi=0$, there is no magnetic field in the system to break the time-reversal symmetry and, at weak coupling, the system is a semimetal, not a topological insulator. Once time-reversal symmetry is broken ($0 < \phi < \pi$), a topological insulator is observed for small V . There is a topological transition from the topological insulator, and this coincides with a first-order

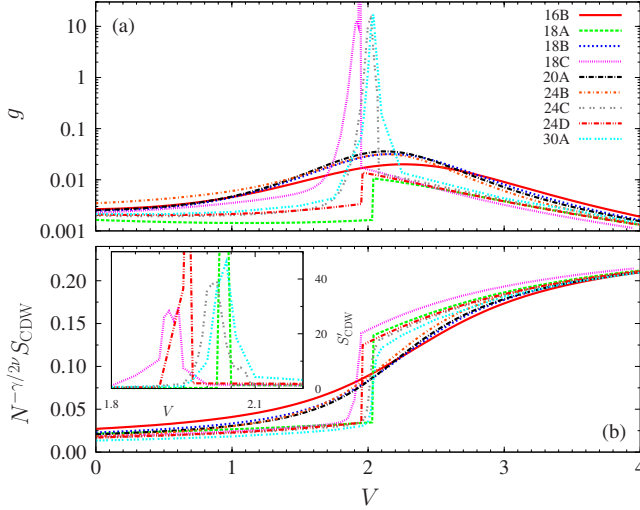


FIG. 8. (Color online) (a) Fidelity metric g as a function of interaction strength for various clusters with parameters $t_1=1.0$, $t_2=0.3$, $\phi=\pi/4$, and $\delta V=10^{-4}$. (b) Scaled CDW structure factor $N^{-\gamma/2\nu} S_{\text{CDW}}$ for the same parameters (shown for $\eta=0$ and $\gamma/\nu=2$). All clusters that contain the zone corner ($\mathbf{k}=\mathbf{K}$) as a valid k point exhibit a sharp, first-order transition at $V_c \approx 2.0$. Without this k point, a smooth, continuous transition is observed. The inset shows the first derivative of the structure factor. The discontinuity (i.e., the peak) marks the transition point.

quantum phase transition to a topologically trivial Mott insulator. Furthermore, we note that the topological phase is strongest at $\phi=\pi/2$.

B. Hard-core bosons

Next, we examined the properties of the Haldane model with hard-core bosons at half filling and nearest-neighbor repulsive interactions, to check whether there are phases with

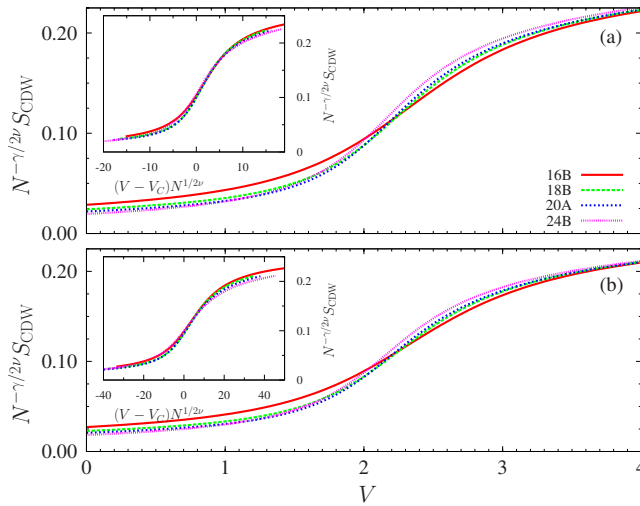


FIG. 9. (Color online) Scaled structure factor $N^{-\gamma/2\nu} S_{\text{CDW}}$ for (a) $z=1$ and $\gamma/\nu=1.96$ ($\eta=0.04$) and (b) $z=2$ and $\gamma/\nu=2$ ($\eta=0$). In both cases, the transition point is found to be $V_c=2.1 \pm 0.1$. In the insets, the horizontal axis is scaled as well, leading to the collapse of all data points into a single curve.

nontrivial topological properties. We are motivated by the fact that in many instances hard-core bosons and spinless fermions are known to have similar properties. In one dimension, one can use the Jordan-Wigner transformation to map one onto the other, i.e., there is a one-to-one correspondence between them. In higher dimensions, one can also expect some similarities. For example, a simple band-structure calculation shows that, at half filling, the ground state of non-interacting fermions on a hypercubic lattice in the presence of a staggered potential M , like the one in Eq. (1), is metallic for $M=0$ and becomes insulating for any nonzero value of M . For hard-core bosons, on the other hand, one has a superfluid (Bose-Einstein condensed) phase for $M < M_c$ and an insulator phase for $M > M_c$,^{54,55} i.e., both models have equivalent ground-state phases. The only difference in this case is that for spinless fermions the metal-insulator transition always occurs at $M_c=0$ while for hard-core bosons the superfluid-insulator transition occurs at a finite value of M_c , which depends on the dimensionality of the system ($M_c=0$ in one dimension, as expected from the exact mapping). Hence, similar physics as discussed in Sec. IV A for spinless fermions would not be unexpected in hard-core boson systems, where, of course, equivalent phases may just appear for different ranges of values of the Hamiltonian parameters.

However, in Fig. 10, we show that this is not the case. For small interaction strengths, the system is a superfluid with essentially no edge current. As V is increased, the system becomes an insulator simultaneously on the edge and in the bulk, indicating a direct transition to the topologically trivial Mott insulator. This Mott insulating state, like the spinless fermion model, exhibits a circulating current on the edge and a depletion of the states in the bulk of the upper band at intermediate coupling strengths. Here the edge currents in the insulating state are larger than for spinless fermions and consequently vanish at larger interaction strengths.

To determine the nature of the phase transition to the CDW phase we examined the fidelity metric and CDW structure factor for various system sizes. The peak in the fidelity metric [Fig. 11(a)] grows with the system size, which is an indicator of a second-order phase transition. Unlike the spinless fermion case in Sec. IV A, the universality class of the transition is unclear. We have performed scaling analysis of the structure factor for both Ising and XY universality classes with dimension $d+z$. The critical exponents for Ising and XY scaling are similar in 3D and identical in 4D and above (the upper critical dimension of both models is 4). Because these exponents are similar and finite-size effects are present in our calculations, we cannot determine which universality class, if any, is the appropriate one. To illustrate this, we show the structure factor rescaled by a factor of $N^{-\gamma/2\nu}$ in Figs. 11(b)–11(d) for 3D Ising, 3D XY,⁵⁶ and 4D Ising/XY, respectively. There is no discernible difference between the three cases. The curves in $N^{-\gamma/2\nu} S_{\text{CDW}}$ versus V for all three cases cross at roughly the same interaction strength ($V_c=3.27 \pm 0.05$ in 3D and $V_c=3.28 \pm 0.05$ in 4D) and the crossing point coincides with the peak in the fidelity metric. Moreover, when plotting $N^{-\gamma/2\nu} S_{\text{CDW}}$ versus $(V-V_c)N^{1/2\nu}$ (see Fig. 11 insets), all the resulting curves almost lie on top of each other. A more detailed study of this model will be presented in future work.³⁶

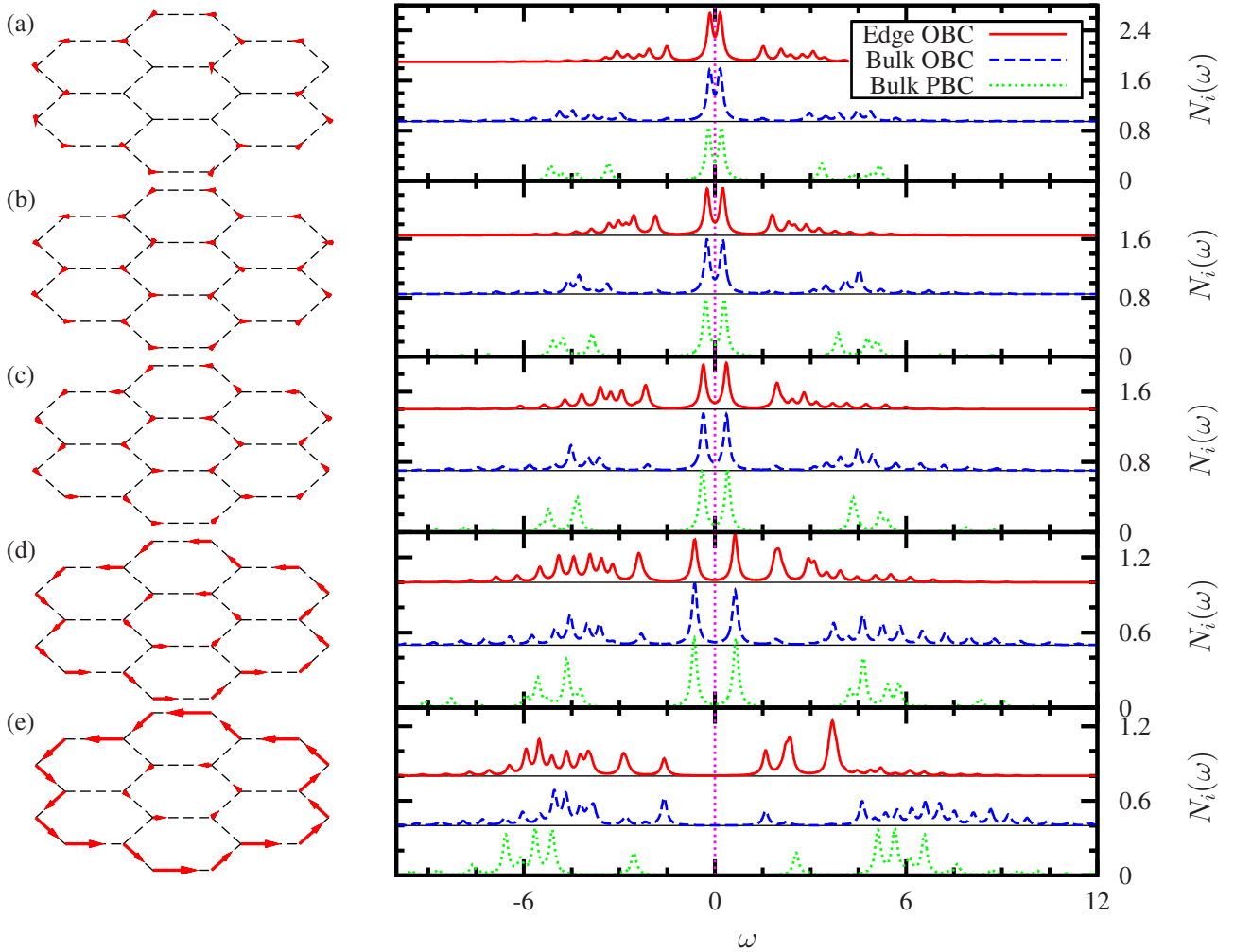


FIG. 10. (Color online) Nearest-neighbor currents (left) for hard-core bosons on a 24-site cluster with OBC, $t_1=1.0$, $t_2=0.3$, $\phi=\pi/4$, and interaction strengths (a) $V=0$, (b) $V=1$, (c) $V=2$, (d) $V=3$, and (e) $V=4$. Local density of states (right) for the edge (OBC) and the bulk (shown for both OBC and PBC). The zeros of $N_{\text{edge}}(\omega)$ and $N_{\text{bulk,OBC}}(\omega)$ are shifted upward for clarity, and the frequency is shifted so that the chemical potential (dashed vertical line) is at $\omega=0$.

V. SUMMARY

In this paper, we have presented the exact nonperturbative study of strong correlation effects in topological insulators. We showed that the clusters that can be studied with the Lanczos algorithm are sufficiently large to identify a topological insulator, clearly distinguishing that the edge states are conducting and the bulk states are insulating. For spinless fermions in the Haldane model with repulsive nearest-neighbor interactions, we found that for weak interaction strengths the system is a topological insulator with circulating edge currents. For large interaction strengths, the system is a topologically trivial CDW insulator. By using the fidelity metric and the CDW structure factor, we showed that the choice of the cluster is significant and that clusters must have a reciprocal space that incorporates the zone corner of the Brillouin zone as a valid k point. For these clusters, we have observed that the transition from the topological insulator to the topologically trivial CDW insulator is first order.

We also investigated the properties of the Haldane model with hard-core bosons at half filling and $\phi=\pi/4$. Here we

found that the bosons are in a superfluid phase for weak interaction strengths and a Mott insulator for large interaction strengths. The growth of the fidelity metric with system size is consistent with a second-order phase transition but scaling of the CDW structure factor cannot distinguish whether the universality class, if any, is Ising or XY. Additionally, no signature of topological order is present in this system. However, this model exhibits interesting critical behavior with a phase diagram that is currently being investigated.³⁶

We note there that the interacting Haldane model by no means exhausts all possible types of interacting lattice Hamiltonians, which may show interesting interplay of strong correlations and topological textures but it rather represents the simplest case where the asymptotic regimes are well understood. Therefore, it is conceivable that other models may host even more interesting transitions and phases such as topological Mott insulators, which would represent the lattice analogs of fractional quantum Hall states. Some candidate states of this sort were previously discussed in Refs. 57–59, however no convincing evidence for their exis-

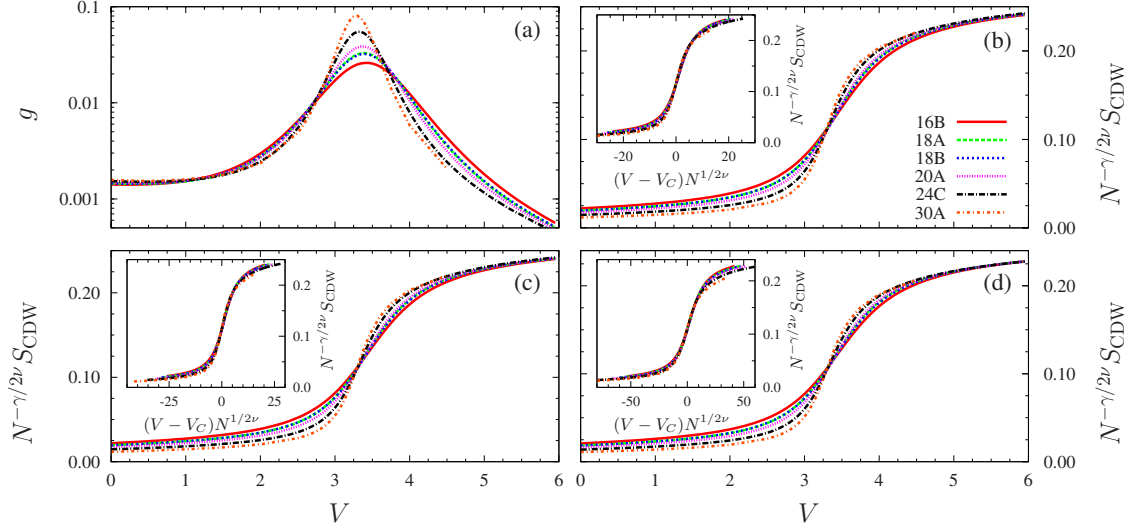


FIG. 11. (Color online) (a) Fidelity metric g as a function of interaction strength for hard-core bosons in various clusters with parameters $t_2=0.3$, $\phi=\pi/4$, and $\delta V=10^{-4}$. [(b)–(d)] Scaled CDW structure factor $N^{-\gamma/2\nu} S_{CDW}$ for (b) 3D Ising ($z=1$), (c) 3D XY ($z=1$), and (d) 4D Ising/XY ($z=2$). All of the curves intersect at the critical point $V_c=3.27\pm 0.05$ in (b) and (c) and $V_c=3.28\pm 0.05$ in (d). In the insets of (b)–(d), the horizontal axis is also rescaled and all of the data points collapse into a single curve.

tence has been found in any model. We conclude by pointing out that our work has important consequences for the studies of topological insulating states in interacting lattice systems because it demonstrates explicitly that most hallmark features of topological insulators survive in small systems, which can be analyzed using unbiased exact diagonalization methods and could be realized in experiments with trapped ions or ultracold gases in optical lattices.⁶⁰

ACKNOWLEDGMENTS

This research was supported by NSF through JQI-PFC (C.N.V., K.S., and V.G.), U.S. Office of Naval Research (C.N.V. and M.R.), and USARO (V.G.). C.N.V. thanks C.-C. J. Wang, E. Khatami, and K. Mielson for useful input.

APPENDIX: CLUSTER SELECTION

It is common in the Lanczos literature to diagonalize clusters with $L\times L$ sites in addition to other square clusters which completely cover the lattice.⁶¹ For a honeycomb lattice, we generally follow a similar prescription of choosing a parallelogram or “tilted rectangle” to describe the cluster. These vectors can be written in terms of the basis vectors \mathbf{a}_1 and \mathbf{a}_2 , shown in Fig. 12, that describe the underlying lattice

$$\begin{aligned} \mathbf{A}_1 &= m_1 \mathbf{a}_1 + m_2 \mathbf{a}_2, \\ \mathbf{A}_2 &= n_1 \mathbf{a}_1 + n_2 \mathbf{a}_2, \end{aligned} \quad (\text{A1})$$

where m_1 , m_2 , n_1 , and n_2 are integers. In Fig. 12, we explicitly show the shape of the clusters used in this work. Note that some of these clusters do *not* have all of the symmetry properties of the bulk. The lone exception to choosing a parallelogram to tile the lattice is the cluster designated 24A. This hexagon-shaped cluster can tile the lattice and retains its

complete symmetry. It is the only cluster studied with open boundary conditions.

As mentioned in the main text above, it is crucial that one distinguish between two different types of clusters, which depend on whether $K=(2\pi/3, 2\pi/\sqrt{3})$ is a valid point in reciprocal space. For this purpose, we provide a necessary and sufficient condition for the K point to be a valid momentum point,

$$\begin{aligned} \alpha_1 &= 2m_1/3 - m_2/3 \in \mathbb{Z}, \\ \alpha_2 &= 2n_1/3 - n_2/3 \in \mathbb{Z}. \end{aligned} \quad (\text{A2})$$

If both α_1 and α_2 for a particular cluster are integers, then K

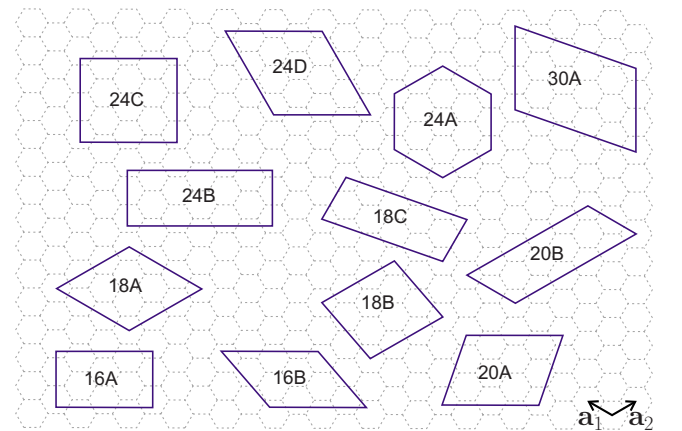


FIG. 12. (Color online) Illustration of different clusters. Only the 18A, 18C, 24C, 24D, and 30A clusters contain the zone corner as a valid k point. The 24A cluster was studied with both open and periodic boundary conditions. The basis vectors for the lattice are shown in the bottom right of the figure.

is a valid point in the reciprocal space for that cluster. The number of sites in a cluster is $N=2|m_1n_2-m_2n_1|$ and it can be easily checked this condition can only be satisfied when the number of sites are $6l$, where l is a positive integer. For the

clusters we studied, only clusters of $N=18, 24$, and 30 sites can contain K point as a momentum point. Notice that a different choice of \mathbf{a}_1 and \mathbf{a}_2 will change the condition described in Eq. (A2).

- ¹F. D. M. Haldane, *Phys. Rev. Lett.* **61**, 2015 (1988).
- ²C. L. Kane and E. J. Mele, *Phys. Rev. Lett.* **95**, 146802 (2005).
- ³B. A. Bernevig, T. L. Hughes, and S.-C. Zhang, *Science* **314**, 1757 (2006).
- ⁴L. Fu, C. L. Kane, and E. J. Mele, *Phys. Rev. Lett.* **98**, 106803 (2007).
- ⁵J. E. Moore and L. Balents, *Phys. Rev. B* **75**, 121306 (2007).
- ⁶R. Roy, *Phys. Rev. B* **79**, 195321 (2009).
- ⁷X.-L. Qi, T. L. Hughes, and S.-C. Zhang, *Phys. Rev. B* **78**, 195424 (2008).
- ⁸R. Li, J. Wang, X.-L. Qi, and S.-C. Zhang, *Nat. Phys.* **6**, 284 (2010).
- ⁹G. E. Volovik, *JETP Lett.* **91**, 55 (2010).
- ¹⁰Z. Wang, X.-L. Qi, and S.-C. Zhang, arXiv:1004.4229 (unpublished).
- ¹¹S. Raghu, X.-L. Qi, C. Honerkamp, and S.-C. Zhang, *Phys. Rev. Lett.* **100**, 156401 (2008).
- ¹²K. Sun, H. Yao, E. Fradkin, and S. A. Kivelson, *Phys. Rev. Lett.* **103**, 046811 (2009).
- ¹³D. Pesin and L. Balents, *Nat. Phys.* **6**, 376 (2010).
- ¹⁴M. Dzero, K. Sun, V. Galitski, and P. Coleman, *Phys. Rev. Lett.* **104**, 106408 (2010).
- ¹⁵S. Rachel and K. Le Hur, *Phys. Rev. B* **82**, 075106 (2010).
- ¹⁶J. Wen, A. Rüegg, C.-C. Joseph Wang, and G. A. Fiete, *Phys. Rev. B* **82**, 075125 (2010).
- ¹⁷R. Blankenbecler, D. J. Scalapino, and R. L. Sugar, *Phys. Rev. D* **24**, 2278 (1981).
- ¹⁸J. E. Hirsch, *Phys. Rev. B* **31**, 4403 (1985).
- ¹⁹E. Y. Loh, J. E. Gubernatis, R. T. Scalettar, S. R. White, D. J. Scalapino, and R. L. Sugar, *Phys. Rev. B* **41**, 9301 (1990).
- ²⁰C. Lanczos, *J. Res. Natl. Bur. Stand.* **45**, 255 (1950).
- ²¹J. K. Cullum and R. A. Willoughby, *Lanczos Algorithms for Large Symmetric Eigenvalue Computations: Theory* (Birkhäuser, Boston, 1985), Vol. 1.
- ²²P. Zanardi and N. Paunković, *Phys. Rev. E* **74**, 031123 (2006).
- ²³W.-L. You, Y.-W. Li, and S.-J. Gu, *Phys. Rev. E* **76**, 022101 (2007).
- ²⁴P. Buonsante and A. Vezzani, *Phys. Rev. Lett.* **98**, 110601 (2007).
- ²⁵S. Chen, L. Wang, S.-J. Gu, and Y. Wang, *Phys. Rev. E* **76**, 061108 (2007).
- ²⁶J. D. Bodyfelt, M. Hiller, and T. Kottos, *EPL* **78**, 50003 (2007).
- ²⁷L. Campos Venuti and P. Zanardi, *Phys. Rev. Lett.* **99**, 095701 (2007).
- ²⁸L. Campos Venuti, M. Cozzini, P. Buonsante, F. Massel, N. Bray-Ali, and P. Zanardi, *Phys. Rev. B* **78**, 115410 (2008).
- ²⁹S. Garnerone, N. T. Jacobson, S. Haas, and P. Zanardi, *Phys. Rev. Lett.* **102**, 057205 (2009).
- ³⁰S.-J. Gu and H.-Q. Lin, *EPL* **87**, 10003 (2009).
- ³¹M. Rigol, B. S. Shastry, and S. Haas, *Phys. Rev. B* **80**, 094529 (2009).
- ³²Q. Niu, D. J. Thouless, and Y.-S. Wu, *Phys. Rev. B* **31**, 3372 (1985).
- ³³K. Ishikawa and T. Matsuyama, *Nucl. Phys. B* **280**, 523 (1987).
- ³⁴G. E. Volovik and V. M. Yakovenko, *J. Phys.: Condens. Matter* **1**, 5263 (1989).
- ³⁵E. Sonin, *Phys. Rev. B* **82**, 113307 (2010).
- ³⁶C. N. Varney, K. Sun, V. Galitski, and M. Rigol (unpublished).
- ³⁷G. Binnig and H. Rohrer, *Rev. Mod. Phys.* **59**, 615 (1987).
- ³⁸E. Dagotto, *Rev. Mod. Phys.* **66**, 763 (1994).
- ³⁹E. R. Gagliano and C. A. Balseiro, *Phys. Rev. Lett.* **59**, 2999 (1987).
- ⁴⁰E. R. Gagliano and C. A. Balseiro, *Phys. Rev. B* **38**, 11766 (1988).
- ⁴¹M. Rigol and B. S. Shastry, *Phys. Rev. B* **77**, 161101 (2008).
- ⁴²S. Wessel, *Phys. Rev. B* **75**, 174301 (2007).
- ⁴³K. Sun and E. Fradkin, *Phys. Rev. B* **78**, 245122 (2008).
- ⁴⁴M. Cheng, K. Sun, V. Galitski, and S. Das Sarma, *Phys. Rev. B* **81**, 024504 (2010).
- ⁴⁵N. Read and D. Green, *Phys. Rev. B* **61**, 10267 (2000).
- ⁴⁶H.-D. Chen, B. Wang, and S. Das Sarma, *Phys. Rev. B* **81**, 235131 (2010).
- ⁴⁷A. Kitaev, *Ann. Phys.* **321**, 2 (2006).
- ⁴⁸F. D. M. Haldane, *Phys. Rev. Lett.* **93**, 206602 (2004).
- ⁴⁹N. Nagaosa, J. Sinova, S. Onoda, A. H. MacDonald, and N. P. Ong, *Rev. Mod. Phys.* **82**, 1539 (2010).
- ⁵⁰S. Sachdev, *Quantum Phase Transitions* (Cambridge University Press, Cambridge, UK, 1999).
- ⁵¹B. Cowan, *Topics in Statistical Mechanics* (Imperial College Press, London, 2005).
- ⁵²R. K. Pathria, *Statistical Mechanics*, 2nd ed. (Butterworth-Heinemann, Oxford, 1996).
- ⁵³P. H. Lundow and K. Markström, *Phys. Rev. E* **80**, 031104 (2009).
- ⁵⁴I. Hen and M. Rigol, *Phys. Rev. B* **80**, 134508 (2009).
- ⁵⁵I. Hen, M. Iskin, and M. Rigol, *Phys. Rev. B* **81**, 064503 (2010).
- ⁵⁶M. Hasenbusch and T. Török, *J. Phys. A* **32**, 6361 (1999), and references therein.
- ⁵⁷D.-H. Lee and J. M. Leinaas, *Phys. Rev. Lett.* **92**, 096401 (2004).
- ⁵⁸A. Seidel, H. Fu, D.-H. Lee, J. M. Leinaas, and J. Moore, *Phys. Rev. Lett.* **95**, 266405 (2005).
- ⁵⁹A. A. Burkov, *Phys. Rev. B* **81**, 125111 (2010).
- ⁶⁰I. Bloch, J. Dalibard, and W. Zwerger, *Rev. Mod. Phys.* **80**, 885 (2008).
- ⁶¹D. D. Betts, S. Matsui, N. Vats, G. E. Stewart, *Can. J. Phys.* **74**, 54 (1996).